[Henry Ford Hospital Medical Journal](https://scholarlycommons.henryford.com/hfhmedjournal)

Volume 33
Number 2 *Medical Imaging 1985*

Article 12

6-1985

Applications of Magnetic Resonance Imaging in Clinical Urology

Barbara A. Demas

Hedvig Hricak

Henry Ford Hosp Med J
Vol 33, Nos 2 and 3, 1985

Applications of Magnetic Resonance Imaging in Clinical Urology

Barbara E. Demas, MD,* and Hedvig Hricak, MD†

During the past two years, the value of magnetic resonance imaging (MRI) in the diagnosis and staging of a variety of urologic neoplasms has been demonstrated, and the ability of MRI to determine sites of renal obstruction and causes of posttransplant renal failure have been reported. Its excellent soft-tissue contrast resolution has allowed accurate delineation of regional anatomy in the kidney, prostate gland, urinary bladder, urethra, uterus, and vagina. The importance of MRI in the urologic diagnosis is expected to increase as clinical imaging systems become widely available.

Experience of two years in clinical application of magnetic resonance imaging (MRI) techniques has demonstrated the particular value of MR assessment of anatomy and pathology of the genitourinary tract. MR images provide unique information regarding the state of hydration and function of both native and transplanted kidneys; the site of origin and the anatomic extent of urologic tumors; the site, cause, and duration of ureteral obstruction; and the relationship of extrarenal pathologic processes to renal and adrenal structures. Unparalleled contrast resolution makes MRI superior to any other imaging modality in the evaluation of anatomic abnormalities in the pelvis. While the potential of MRI is only beginning to be realized, the value of these techniques in the diagnosis of urologic disease is readily evident. The physical principles of MRI have been summarized in a number of sources (1-3) and will not be discussed here.

Normal Anatomy of the Kidneys and Adrenal Glands

The appearance of the normal kidneys in MR images varies with the state of hydration and the selection of imaging parameters (4). The signal intensity of renal cortex is higher than that of renal medulla, and the corticomedullary border is distinct when well-hydrated kidneys are evaluated using spin-echo techniques and short TR values (0.5 to 1.0 sec) (Fig 1). Corticomedullary differentiation is lost with dehydration and in a variety of medical diseases and is undetectable if long TR values are used (1.5 to 2.0 sec). When filled with urine, a relatively pure fluid with long T1 and T2 values, the pelvocalyceal structures are seen as tubular structures of low signal intensity on images obtained using short TR values. The signal intensity of intraluminal urine increases slightly with TR prolongation. Renal sinus and perirenal fat with short T1 and T2 values appear of high signal intensity in images obtained using either short or long TR values. Striated muscles appear of medium signal intensity in images obtained using TR values. The signal intensity decreases with TE prolongation. The renal vessels, aorta, and inferior vena cava appear as tubular structures devoid of intramural signal if the rate of blood flow is normal. The adrenal glands appear in transaxial images as bilobed structures, their limbs approximately equaling the thickness of the diaphragmatic crura. Images obtained using short TR values show the adrenal cortex to be of higher signal intensity than the medulla. The corticomedullary differentiation and the distinction of adrenal glands from surrounding retroperitoneal fat are decreased when TR values are increased.

Evaluation of Genitourinary Pathology

Inflammatory disease

The appearance of the pyelonephritic kidney in MR images reflects the extensive interstitial inflammatory change and intrarenal edema seen at pathologic evaluation. The kidney may appear swollen in contour, and the distinction between cortex and medulla is lost (4-6). This loss is caused by an increase of the T1 values of cortex, probably due to exudation of fluid from the cortical capillary bed. The production of an intrarenal abscess causes the appearance of a localized fluid collection; the signal intensity of abscess fluid varies with the protein and content of the fluid.

Obstructive disease

Renal stones do not produce a signal in MR images because they lack mobile protons. They may be detected, however, as areas of signal void within the renal parenchyma, pelvocalyceal structures, or ureters. Masses compressing the ureters vary in appearance depending on their tissue content; ureteral obstruction is detectable when the ureter or pelvocalyceal structures are dilated (Fig 2). In cases of acute ureteral obstruction the renal parenchyma may be of normal appearance. However, when there is chronic obstruction, the normal corticomedullary border is not visible (7).

Submitted for publication: May 29, 1985

Accepted for publication: June 17, 1985

*Department of Radiology, University of California School of Medicine

†Department of Radiology, University of California School of Medicine. Formerly from Department of Diagnostic Radiology, Henry Ford Hospital

Reprints not available

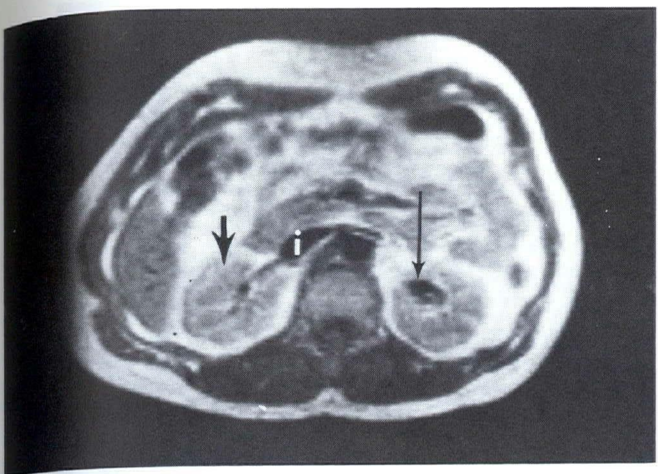

Fig 1
Transaxial MR image (SE TR = 1.0 sec, TE = 28 msec) demonstrates normal renal anatomy. Boundary between high-signal-intensity renal cortex and low-signal-intensity renal medulla is clearly seen (large arrow). Urine-filled renal pelvis is visible in left renal hilum (small arrow). Renal veins, inferior vena cava (i), and aorta are demonstrated as tubular structures devoid of intraluminal signal.

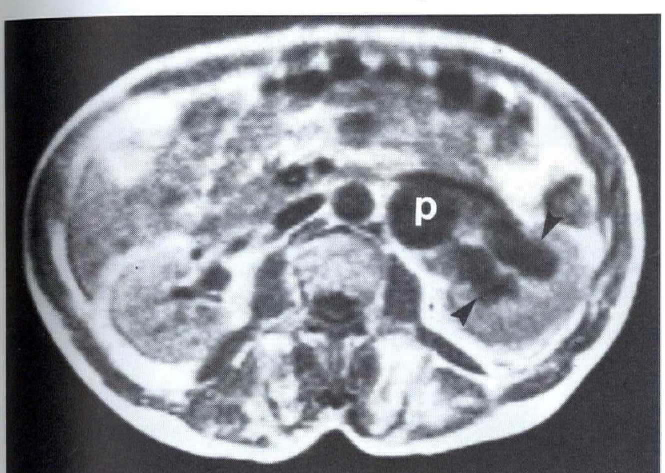

Fig 2
Transaxial MR image (SE TR = 1.0 sec, TE = 28 msec) demonstrates dilated fluid-filled renal pelvis (p) and dilated calyces (arrows) in this patient with chronic ureteral obstruction.

Cystic disease

Both simple renal cysts and polycystic renal disease may be evaluated using MR imaging. Cysts differ in appearance with alterations in fluid protein content. Simple cysts are round, well circumscribed, and of low signal intensity in short TR images (6). Their signal intensity increases somewhat with TR prolongation. Hemorrhagic or infected cysts may appear of high signal intensity in short and long TR images due to T1 shortening by elevated protein content. The accuracy of MRI in differentiating cystic from solid masses is still to be established.

Neoplasms

Initial evaluation of the accuracy of MRI has shown it to be comparable to state-of-the-art CT in assisting in the diagnosis and staging of renal cell carcinoma (8). Renal cell carcinomas appear in MR images as masses of variable signal intensity that distort renal contours or intrarenal architecture (8-10). Small intrarenal tumors may be difficult to detect. These tumors are heterogeneous in signal pattern and in change of signal intensity with TR and TE prolongation (Fig 3). MRI readily demonstrates tumor vascularity and accurately assesses patency of the renal veins and inferior vena cava. MRI has exceeded CT in ease and accuracy of detection of perivascular adenopathy in our experience. The ability of MRI to generate images directly in the sagittal plane has been helpful in evaluating the presence or absence of extension of tumor into the adjacent liver, spleen, and paraspinous musculature.

Adrenal carcinomas, pheochromocytomas, and adrenal metastases have been detected by MR techniques but have been studied only in small numbers to date. In our experience, these lesions have produced masses of varying size, generally of homogeneous signal intensity that increases with increase of TR, and they have lacked the extensive tumor vascularity of renal cell carcinomas. Hepatic metastases from adrenal carcinomas have appeared as sites of relatively high signal intensity compared with that of surrounding liver tissue, and they have increased in relative intensity with TE prolongation.

Renal transplants

MRI is valuable in the assessment of possible renal transplant rejection, and in the presence of appropriate clinical history, MR images can be used to differentiate rejection from cyclosporin nephrotoxicity. The normally functioning, well-hydrated transplant kidney has the imaging characteristics described for the native kidney. A transplanted kidney being rejected will not demonstrate a clear corticomedullary border in short TR images (11). Associated inflammation may cause a decrease in signal intensity of surrounding fat and an increase in intensity of underlying psoas muscle. Decreased renal function caused by cyclosporin toxicity will be associated with no detectable abnormalities of renal morphology. Patency of renal vessels, dilation of collecting structures, and peritransplant fluid collections can be assessed with MRI as well.

Normal Anatomy of the Pelvis

The excellent soft-tissue contrast resolution and the capability of obtaining transaxial, coronal, and sagittal images make MRI the modality of choice in evaluating a variety of structural abnormalities of the pelvis (12,13). Each imaging plane offers useful information depending on the type of anatomy being studied.

MR images allow distinction of the bladder wall from intraluminal urine when the spin-echo technique, using long TR and TE values, is employed. In the male pelvis, transaxial,

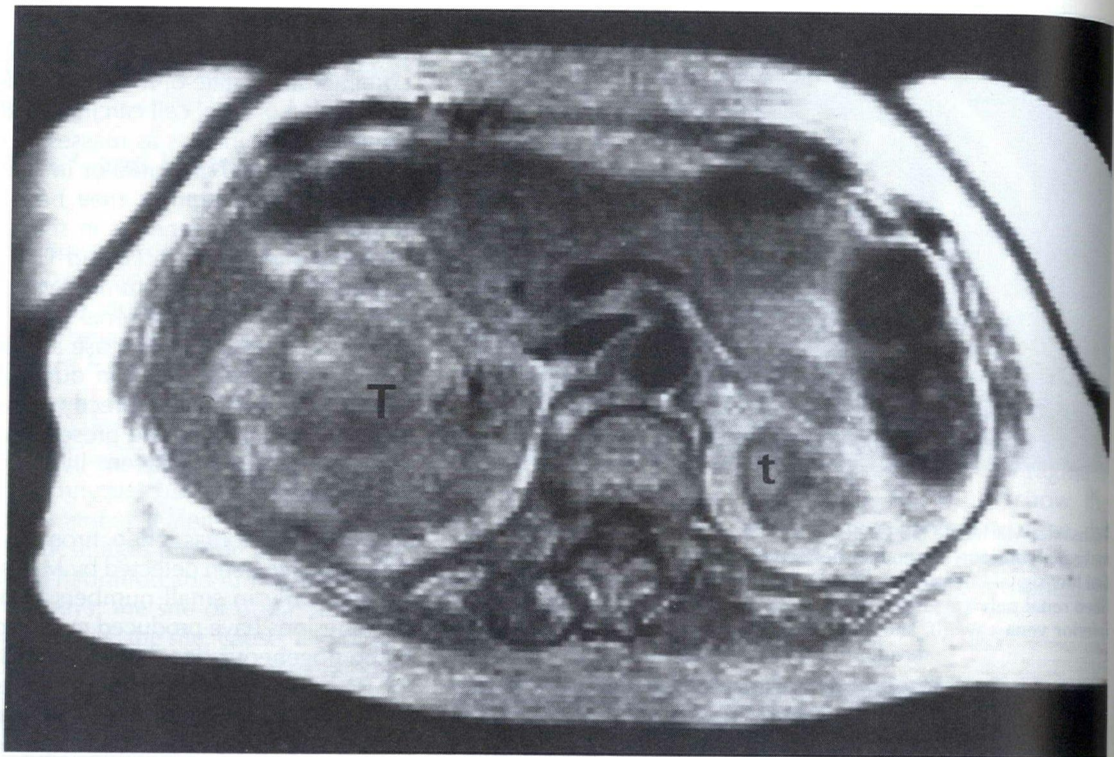

Fig 3
Transaxial MR image (SE TR = 2.0 sec, TE = 28 msec) shows large right-sided renal cell carcinoma (T) and smaller coincident renal cell carcinoma (t) in left kidney. Tumors are heterogeneous in signal intensity.

sagittal, and coronal images clearly display the ductus deferens and seminal vesicles posterior to the urinary bladder near its base. Short TR images facilitate visual separation of the medium-signal-intensity seminal vesicles from surrounding high-signal-intensity pelvic fat; prolongation of TR to 2.0 sec results in increased signal intensity from seminal vesicles and makes this contrast less apparent.

Coronal and sagittal images make possible evaluation of the relationship of the prostate gland to the bladder base (Fig 4). The central zone of the prostate is generally of lower signal intensity than the peripheral zone. Denovillier's fascia, which separates the prostate gland from the rectum, is imaged as a low-intensity band, the presence of fibrous tissue accounting for the low signal strength. This structure is best evaluated in sagittal plane images as are the membranous, prostatic, and bulbous portions of the urethra.

Axial and coronal images allow demonstration of the relationship between the levatores ani and the prostate gland. The muscles are of lower signal intensity than the immediately adjacent peripheral prostatic zones, and the boundaries between these structures can be easily appreciated.

In the female patient, sagittal images allow evaluation of the relationship of the urethra, vagina, and rectum, as do transaxial views. The corpus uterus and cervix are clearly delineated in sagittal images, and the boundaries between high-signal intensity cyclic endometrium, low-intensity junctional zone, and medium-intensity myometrium are seen when TR or TE values are relatively long (Fig 5).

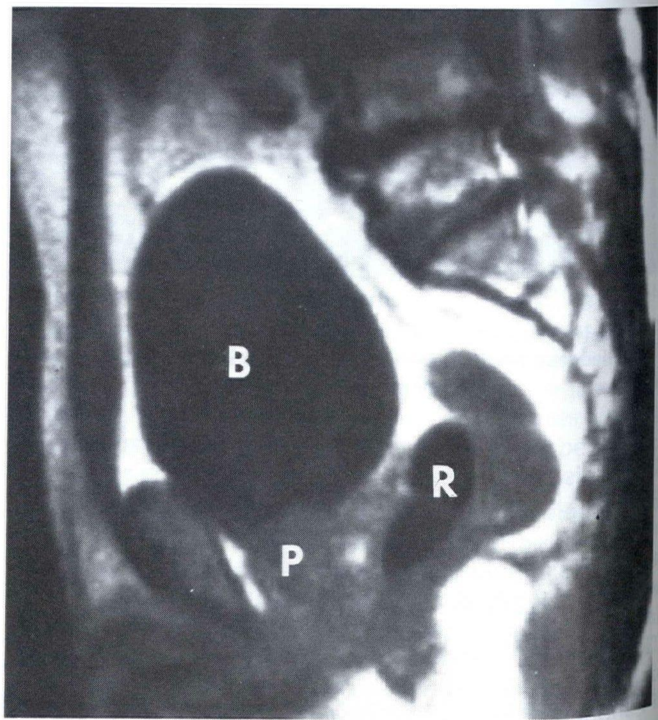

Fig 4
Sagittal MR image (SE TR = 0.5 sec, TE = 28 msec) demonstrates relationship between prostate gland (P), urinary bladder (B), and rectum (R).

Fig 5
Sagittal MR image (SE TR = 1.5 sec, TE = 56 msec) shows normal anatomy of female pelvis. Three layers of corpus uterus (arrow) are distinct. Centrally located high-signal-intensity zone basalis from medium-signal-intensity myometrium. Urinary bladder is slightly distended; urine appears of relatively high signal intensity because TE is relative prolonged.

Evaluation of Pelvic Pathology

Urinary bladder neoplasm

Only a small number of bladder tumors have been imaged to date, but MR images have demonstrated distinct borders between tumors and normal portions of bladder wall, delineated extraluminal and intramural extension of tumor, and revealed invasion of perivesicle fat. Transitional cell tumors have appeared as lobulated masses, often sessile, of higher signal intensity than adjacent bladder wall when long TR and TE values are used (Fig 6). Associated vesicle-wall edema has caused signal intensity higher than that of the visualized tumors. Perivesicle fat infiltration by tumor extension has produced streaky areas of medium to low signal intensity within the normally high-signal-intensity fat. Perivascular adenopathy produces lobular masses adjacent to and sometimes indenting vessels. Enlarged lymph nodes are best separated visually from fat in images obtained using short TR values; such nodes may be more easily separated from pelvic musculature in images obtained using longer TR values.

Prostatic hypertrophy

Benign prostatic hypertrophy appears as prostatic enlargement. Signal intensity is often homogeneous, but heterogeneous high-intensity nodules have been detected. Associated urethral displacement can be demonstrated.

Prostatitis

Inflammatory disease of the prostate gland may produce heterogeneity of signal pattern that is difficult to distinguish from neoplasm in the absence of clinical history (14). Prostatic urethritis may cause periurethral edema and urethral dilatation.

Prostatic neoplasms

Prostatic carcinomas cause alterations in patterns of signal intensity: the gland becomes heterogeneous in appearance with localized or scattered areas of high signal intensity. Extension of disease into the seminal vesicles may cause asymmetric enlargement and increase in signal intensity of these structures and is well evaluated in transaxial and coronal views. Coronal images are valuable in revealing transcapsular extension of tumor into the levator ani muscles; sites of tumor extension cause increase in signal intensity in affected muscle. Adenopathy is most easily assessed in transaxial images. Extension of tumor through Denovillier's fascia into the rectum is best appreciated in sagittal plane images.

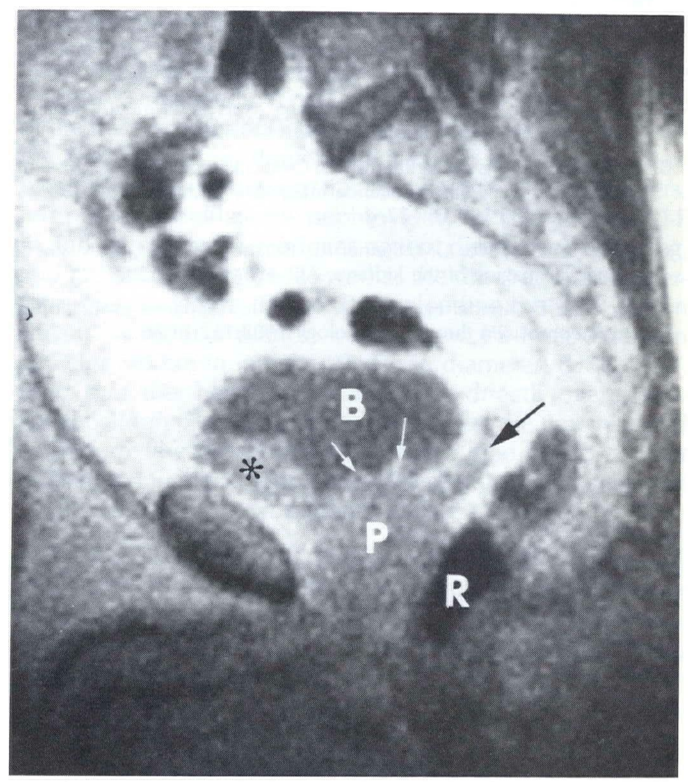

Fig 6
Sagittal MR image (SE TR = 1.0 sec, TE = 28 msec) of male pelvis shows transitional cell carcinoma (*) of bladder (B). Prostate gland (P) and rectum (R) are clearly delineated. Seminal vesicles (arrow) are visible, surrounded by pelvic fat.

Congenital anomalies

Congenital absence of the seminal vesicles has been detected or confirmed with MRI in several instances. Multiplanar images facilitate evaluation of hypoplastic genitourinary organs or of ectopic or dysmorphic structures.

Gynecologic pathology

The ability of MRI to differentiate uterine zonal anatomy is unique. Uterine leiomyomata, endometrial and cervical carcinomas, and extrauterine abnormalities, such as endometriomas and ovarian cysts, have been identified and characterized by MRI. Sagittal images provide information regarding normal and pathologic anatomy of the urethra, vagina, and rectum. Congenital anomalies including vaginal agenesis, cervical stenosis, and uterine and vaginal duplication have been detected in MR images. These findings have assisted in preoperative surgical planning.

In summary, the noninvasive evaluation of genitourinary anatomy and pathology has been greatly facilitated by application of MRI techniques. The excellent soft-tissue contrast resolution and the capability of obtaining images directly in multiple planes have allowed staging of renal and prostatic neoplasms with ease and accuracy. Preliminary results in the evaluation of bladder neoplasms are promising. Assessment of renal transplant function and rejection by MRI holds the promise of being superior to that offered by any other imaging modality. The importance of MRI in the evaluation and management of urologic disease is expected to increase as clinical imagers become more widely available.

References

1. Pykett IL, Newhouse JH, Buonanno FS, et al. Principles of nuclear magnetic resonance imaging. Radiology 1982;143:157-68.
2. Crooks LE, Kaufman L. Basic physical principles. In: Margulis AR, Higgins CB, Kaufman L, Crooks LE, eds. Clinical magnetic resonance imaging. San Francisco: Radiology Research and Education Foundation, 1983:13-24.
3. James TL. Basic nuclear magnetic resonance principles. In: James TL, Margulis AR, eds. Biomedical magnetic resonance. San Francisco: Radiology Research and Education Foundation, 1984:7-22.
4. Hricak H, Crooks LE, Sheldon P, Kaufman L. Nuclear magnetic resonance imaging of the kidney. Radiology 1983;146:425-32.
5. London DA, Davis PL, Williams RD, Crooks LE, Sheldon PE, Gooding CA. Nuclear magnetic resonance imaging of induced renal lesions. Radiology 1983;148:167-72.
6. Leung AWL, Bydder GM, Steiner RE, Bryant DJ, Young IR. Magnetic resonance imaging of the kidneys. AJR 1984;143:1215-29.
7. Thickman D, Kundel H, Biery D. Magnetic resonance evaluation of hydronephrosis in the dog. Radiology 1984;152:113-6.
8. Hricak H, Demas BE, Williams RD, et al. Value of magnetic resonance imaging in diagnosis and staging of renal and perirenal neoplasms. Radiology 1985;54:709-15.
9. Hricak H, Williams RD, Moon KL Jr, et al. Nuclear magnetic resonance imaging of the kidney: Renal masses. Radiology 1983;147:765-72.
10. Choyke PL, Kressel HY, Pollack HM, et al. Focal renal masses: Magnetic resonance imaging. Radiology 1984;152:471-7.
11. Geisinger MA, Risius B, Jordan NL, Zelch MG, Novick AC, George CR. Magnetic resonance imaging of renal transplants. AJR 1984;143:1229-34.
12. Hricak H, Alpers C, Crooks LE, Sheldon PE. Magnetic resonance imaging of the female pelvis: Initial experience. AJR 1983;141:1119-28.
13. Hricak H, Williams RD, Spring DB, et al. Anatomy and pathology of the male pelvis by magnetic resonance imaging. AJR 1983;141:1101-10.
14. Poon PY, McCallum RW, Henkelman M, et al. Magnetic resonance imaging of the prostate. Radiology 1985;154:143-9.